COMPARATIVE ANALYSIS OF WEATHER RADAR SIGNATURES OF *PUTING BELIUNG* IN INDONESIA

Kiki[12], Yonny Koesmaryono[2], Rahmat Hidayat[2], Donaldi S Permana[1], Perdinan[2*]
[1]Agency of Meteorology, Climatology, and Geophysics, Jakarta, Indonesia 10720
[2]Department of Geophysics and Meteorology, IPB University, Jalan Meranti Wing 19 Level 4 Darmaga Campus, Bogor, Indonesia 16680
***E-mail:** perdinan@apps.ipb.ac.id*

Received: July 31, 2025 Reviewed: October 31, 2025 Accepted: January 19, 2026

ABSTRACT

This study presents a comprehensive radar-based analysis of "*Puting Beliung*" (PB), Indonesia's localized tornado phenomenon, using multiple weather radar-derived products. The study performs a comparative analysis across ten PB cases to identify consistent meteorological signatures and variations in tropical storm behavior. Recent data indicate that PB events are increasing in frequency in Indonesia, necessitating improved detection methods. Analysis of ten PB cases using Rainbow software revealed consistently high reflectivity values (35-60 dBZ). While echo patterns were diverse, the hook echo pattern was the most dominant across the observed cases. Physical parameters indicated horizontal wind speeds of 10-30 knots at 4 km altitude, horizontal shear of 5-10 m/s/km, and vertical shear of 1-10 m/s/km. Additionally, spectral width analysis indicated moderate turbulence at a speed of 3 m/s. The Tornadic Vortex Detection (TVD) product detected potential vortex signatures at six locations, with heights ranging from 1.2 to 3.1 km. This study represents the first comprehensive radar product analysis application for PB characterization in Indonesia, establishing CMAX, HWIND, HSHEAR, and TVD as the most effective products for PB detection and monitoring. These findings provide crucial baseline criteria for developing radar-based early warning systems specifically calibrated for Indonesia's tropical environment, which could reduce the socioeconomic impact of PB events through improved detection and prediction capabilities.

Keywords: puting beliung, tornadoes, weather radar, echoes

1. Introduction

Puting beliung (PB) represents a significant extreme weather phenomenon in Indonesia, ranking as the second most frequent natural disaster after floods in recent years [1]. This localized tornado phenomenon is characterized by rotating strong winds originating from Cumulonimbus (Cb) clouds, which touch the ground with a minimum speed of 34.8 knots, and occur quickly [2]. While the official ground-level definition requires speeds of at least 34.8 knots, radar-detected wind speeds at higher altitudes often vary depending on the storm's stage and elevation. Historical data indicated that PB accounted for 21% of disaster events in Indonesia from 1815 to 2014 [3]. PB is often referred to as a localized or weak tornado [4], [5]. This extreme phenomenon is reported to exhibit high frequency in Java Island [6], [7] and has shown an increasing trend in frequency from 2011 to 2016 [7], [8].

The transition season, which is between September and November and between March and May, is said to be the period with the highest incidence of PB in Indonesia throughout the year [6], [7], [9], with the highest frequency per month recorded in January, March, and November [10]. The most common occurrence time of PB is between noon and afternoon, i.e., between 1 p.m. and 3 p.m. local time [10].

Although PB occurs in a relatively narrow area and within a short period [11], the impacts are very destructive. Commonly reported impacts caused by PB include flying roofs, building damage, uprooted trees, fallen electricity poles, and collapsed billboards, which can result in casualties [6]. The economic loss caused by this phenomenon in Central Java province from 1990 to 2011 is estimated to reach up to IDR 280 billion [6]. Psychological impacts in the form of trauma and excessive anxiety have also been reported in PB victims, especially children [12].

Given these impacts, it is crucial to advance the detection and prediction of PB. This study conducts a comparative analysis across ten distinct PB cases occurring in various Indonesian regions to identify universal versus site-specific radar signatures. Unlike previous studies that relied on post-event damage assessments, our research quantitatively characterizes PB through real-time radar observations. While previous studies have established the temporal and spatial patterns of PB occurrence in Indonesia [6], [7],

[10], the systematic analysis of PB signatures using weather radar remains limited. Prior research has employed weather radar products to investigate Puting Beliung occurrences in Indonesia. Notably, Ali et Hidayati [8], reported strong horizontal shear ranging from 6.23 to 10.12 m s^{-1} km^{-1} at 0.5 km altitude, accompanied by rotational patterns and updrafts exceeding 20 knots at low levels (100–200 m), despite moderate turbulence values (1.75–2.05 m s^{-1}) in several PB cases in Lampung, East Java, and Bali region. Other studies in southern Brazil have reported that tornadic events can occur in low-topped storms with moderate reflectivity, differing from classic supercells. Specifically, Nascimento et al. [13] found that no evident hook echo was observed despite a strong tornado confirmation, attributing this limitation to the long distance between the storm and the radar, combined with the radar beam width. Building upon these foundational studies, our research employs multiple weather radar-derived products to characterize PB signatures, offering a more comprehensive understanding of their formation and evolution. This approach aligns with international best practices in tornado detection, with weather radar being the primary tool [14], [15], while addressing the challenges of monitoring these phenomena in Indonesia's tropical environment.

As the world's largest archipelagic country, Indonesia's position creates distinctive meteorological conditions that may influence the formation of PBs. The interaction between maritime and continental air masses, combined with intense solar heating of land areas, creates strong local convection patterns. The country's location within the Inter-Tropical Convergence Zone (ITCZ) and exposure to multiple monsoon systems generate complex atmospheric dynamics throughout the year. The varied topography, from coastal plains to mountainous regions, can enhance local wind convergence and vertical motion. These unique geographical and meteorological factors may contribute to the distinctive characteristics of PB events compared to tornadoes in other regions, particularly in their rapid development and diverse radar signatures. Understanding these local conditions is crucial for interpreting radar observations and developing effective detection methods.

This study aims to characterize PB events using multiple weather radar-derived products and identify specific radar signatures associated with PB occurrence. By analyzing weather radar-derived products for several PB cases, it is expected that conclusions will be drawn about the general characteristics and unique patterns of PB identified on weather radar products, and that the most effective radar products for PB detection and monitoring will be determined. The results of this research are expected to make a positive contribution to the development and strengthening of an early warning system for PB based on weather radar observations in Indonesia.

2. Data and Methods

The study analyzed ten PB events between 2022 and 2024 across various Indonesian regions using C-Band radar data from BMKG's weather radar network. Raw radar data processing employed Rainbow software version 5.0, with the following specifications as provided in Table 1.

Table 1. Specifications of the weather radars used in the research.

Radar Sites	Max Range (km)	Spatial Res. (m)	Beam Width (deg)	Max Velocity (m/s)	No. of Elevations
Syamsudin Noor Meteorological Station - Banjarmasin	250	250	1	18.585	9
Mobil Cepat Radar Cuaca (MCRC) Kertajati - Majalengka	120	250	1.3	18.585	8
Tebelian Meteorological Station - Sintang	200	1000	0.892	7.9785	10
Depati Amir Meteorological Station - Pangkal Pinang	249	225	0.956	18.585	3
Sultan Mahmud Badaruddin II Meteorological Station - Palembang	240	250	0.95	23.85	9
Juanda Meteorological Station - Sidoarjo	200	500	1	33.125	9
Kualanamu Meteorological Station - Medan	200	250	1	18.585	9
YIA Meteorological Station - Yogyakarta	200	225	0.955	18.585	10
Soekarno Hatta Meteorological Station - Tangerang	200	250	1	18.585	9

Data quality control included removing non-meteorological echoes, which were filtered using the built-in quality control algorithms in the Rainbow 5.0 software. Additionally, signal-to-noise ratio (SNR) was applied, and data below 10 dB were excluded from analysis. Ground clutter suppression using a digital elevation model and clutter map specific to each radar site, and velocity deliasing performed using the Rainbow software's integrated dealiasing algorithm. Table 2 provides information on the 10 selected PB cases. The selection of the 10 PB cases in the study is based on the availability of weather radar data, the distance between the PB event location and the radar site being less than 200 km, and the absence of obstacles between the two locations.

Table 2. Location and time of occurrence of selected PB cases in the study.

	PB events location and time	Radar Sites	Distance between PB event and radar site (km)
1.	South Kalimantan, Hulu Sungai Selatan, Angkinang, 20 June 2022 around 15.00 LT	Syamsudin Noor Meteorological Station - Banjarmasin	89
2.	West Java, Bandung, Rancaekek, 21 Februari 2024 around 15.50 LT	Mobil Cepat Radar Cuaca (MCRC) Kertajati - Majalengka	56
3.	West Kalimantan, Sintang, Tanjung Puri, 16 May 2024 around 16.30 LT	Tebelian Meteorological Station - Sintang	11
4.	South Kalimantan, Banjar, Sungai Tabuk, 15 September 2022 around 13.15 LT	Syamsudin Noor Meteorological Station - Banjarmasin	23
5.	Bangka Belitung Island, Bangka, Belinyu, Gunung Pelawan, 15 October 2022 around 12.30 LT	Depati Amir Meteorological Station - Pangkal Pinang	71
6.	South Sumatra, Muara Enim, Gelumbang, Sukajaya, 30 March 2022 around 13.30 LT	Sultan Mahmud Badaruddin II Meteorological Station - Palembang	49
7.	East Java, Jombang, Megaluh, 17 January 2024 around 15.30 LT	Juanda Meteorological Station - Sidoarjo	64
8.	North Sumatra, Deli Serdang, Percut Sei, Sampali, 7 May 2024 around 13.30 LT	Kualanamu Meteorological Station - Medan	15
9.	Central Java, Cilacap, Nusawungu, Jetis, 23 January 2024 around 06.20 LT	YIA Meteorological Station -Yogyakarta	78
10.	West Java, Indramayu, Tukdana, 24 January 2024 around 16.00 LT	Soekarno Hatta Meteorological Station - Tangerang	185

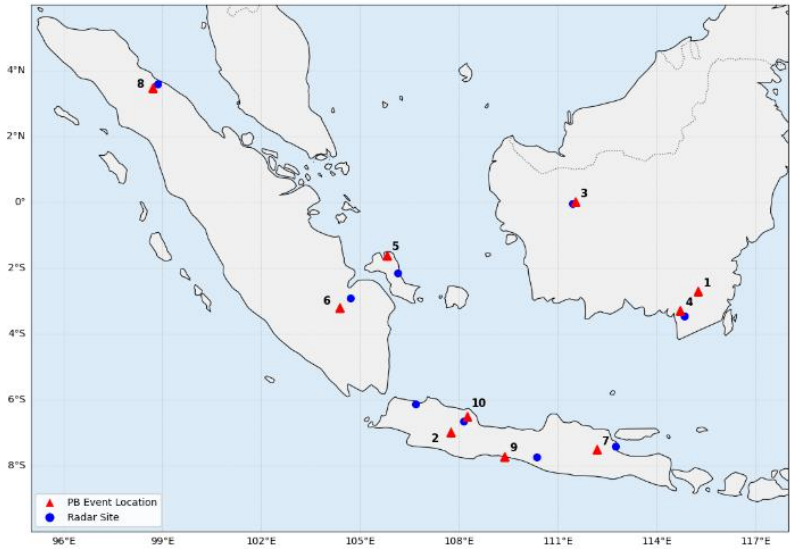

Figure 1. PB event locations and weather radar sites used; red icons represent PB event locations; blue icons represent weather radar sites.

The distance between the PB events and the radar sites in this study varies from 11 km to 185 km, which introduces challenges related to radar beam broadening and Earth's curvature. Consequently, small-scale low-level vortices like PB may not be fully resolved at such distances and lose their fine structural detail. Furthermore, due to the Earth's curvature, the radar beam at 185 km (even at 0.5° elevation) is positioned significantly higher than the ground, potentially missing the lowest part of the vortex. To mitigate this, our analysis of distant cases prioritized vertically integrated products, such as CMAX, while high-resolution products like TVD and Shear, were interpreted with greater caution in cases beyond 100 km. Figure 1 shows the locations of PB events and the weather radar sites used in the study. The study processed the weather radar-derived products using Rainbow software [16], as shown in Table 3, while Figure 2 illustrates the workflow.

Table 3. Weather radar-derived products used in the study.

Products	Description	Definition	Previous Studies
CMAX	Column Maximum	Maximum value of reflectivity in the vertical column of the atmosphere for each horizontal pixel in the radar coverage	[8], [17], [18]
HWIND	Horizontal Wind	Calculation of horizontal wind vectors on a grid within radar coverage with radial velocity data input	[8], [17], [19]
SSA	Storm Structure Analysis	Analyze significant storm structure in radar coverage by integrating reflectivity, velocity, and spectral width scans in the same scan for all elevations or scans	[8]
SPECTRAL WIDTH		Detects atmospheric turbulence	[8], [20]
SHEAR	Hshear & Vshear	Detect horizontal and vertical changes in wind direction and velocity	[8], [21]
TVD	Tornadic Vortex Detection	Analyzing 3-dimensional radial velocity data for identification of Tornado Vortex Signatures (TVS) patterns	[21], [22], [23], [24], [25]

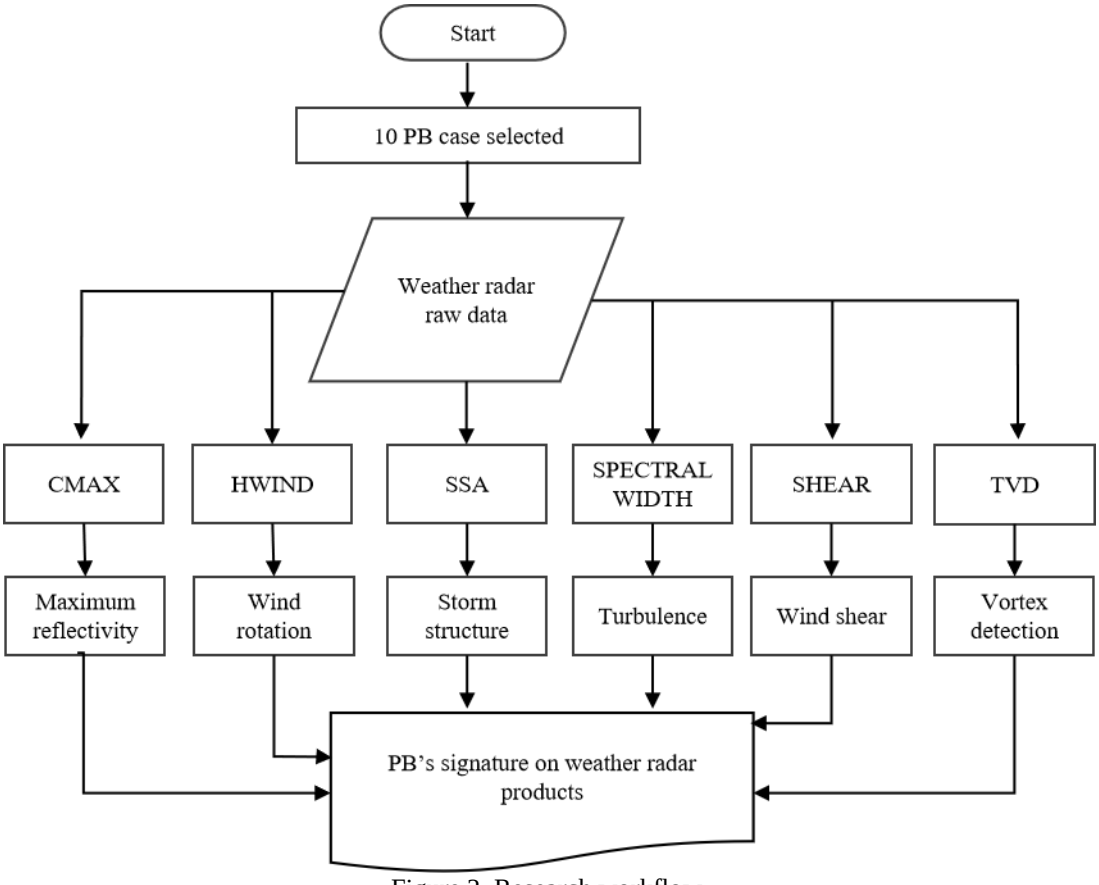

Figure 2. Research workflow.

3. Result and Discussion

PB's signatures on CMAX. Analysis of the PB special features in the 10 case studies of the CMAX product reveals fairly consistent characteristics. All PB cases exhibit high maximum reflectivity values, ranging from 35 to 60 dBZ, during the peak phase of cloud growth, before weakening to 20-40 dBZ and transitioning into stratiform clouds. The duration of growth to decay of this cloud lasts around 30-40 minutes, with a rapid growth to mature phase duration of around 10-20 minutes.

The special characteristics of PB recorded in CMAX products vary, namely in the form of hook echo patterns identified in the PB cases of Sungai Tabuk (Figure 3a), Belinyu (Figure 3b), and bow echo patterns at the Tanjung Puri PB location (Figure 3c). The v-shape pattern was detected in the case of PB Rancaekek (Figure 3d) in two different systems: a single-cell storm at 08:30 UTC and a multi-cell storm at 08:50 UTC. In the case of PB Gelumbang (Figure 3e), the recorded special pattern is a line-type mesoscale convective system (MCS) characterized by elongated cloud clusters moving in the same direction.

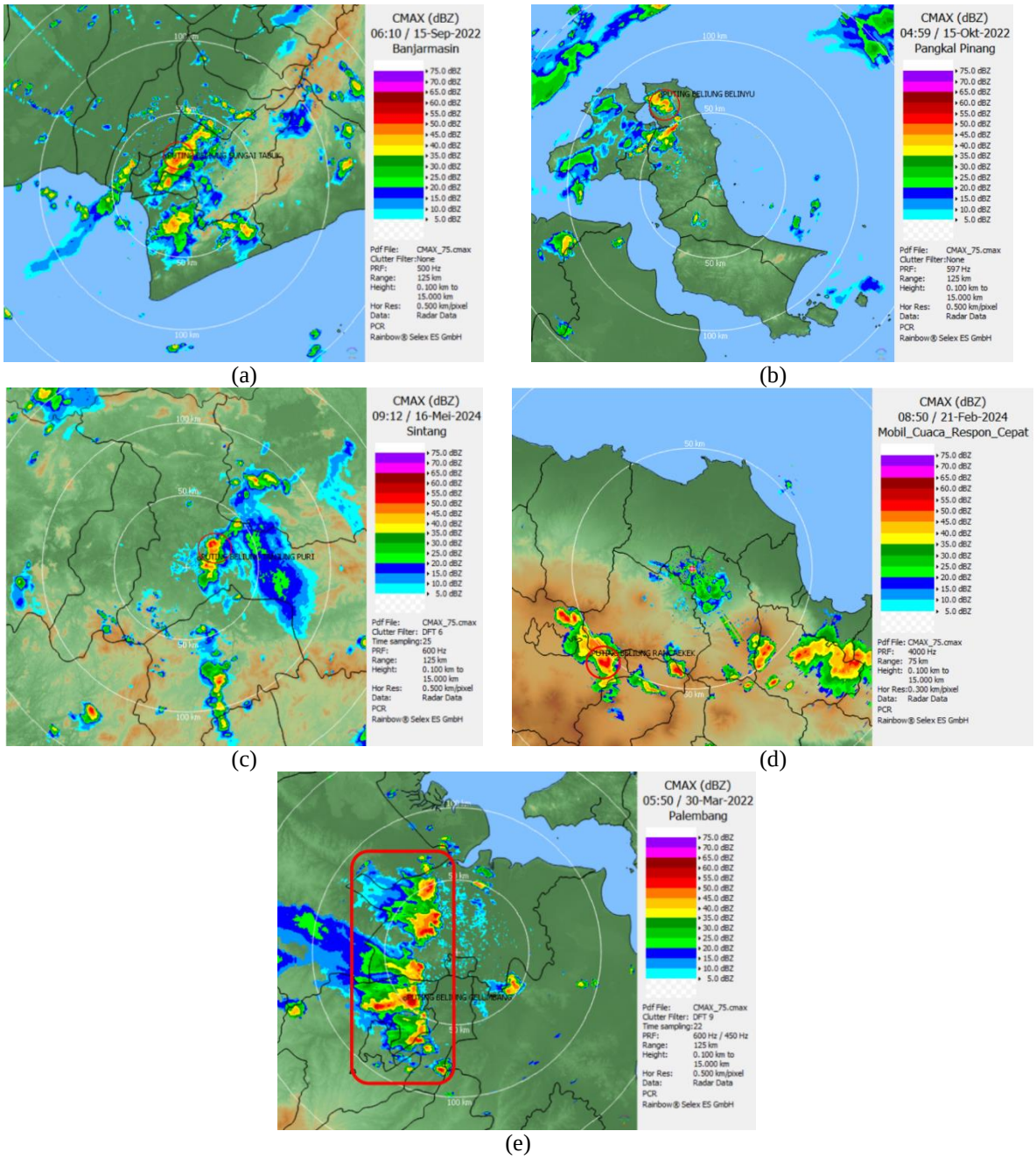

(a) (b) (c) (d) (e)

Figure 3. CMAX images of PB events at (a) Sungai Tabuk, Banjarmasin, South Borneo (b) Belinyu, Bangka Belitung Island (c) Tanjung Puri, Sintang, West Borneo (d) Rancaekek, Bandung, West Java (e) Gelumbang, Palembang, South Sumatra.

Although not all PB events analyzed show the bow or hook echo patterns often associated with PB or tornadoes, all cases show consistency in the characteristics of high reflectivity and short-duration cloud growth. The diversity of specific patterns recorded indicates that PB phenomena in Indonesia can occur in various convective cloud systems and are not limited to one specific pattern. Our findings of hook echo patterns in Indonesian PB events align with observations from Japanese tornadoes, particularly the Fujisawa City (2006) and Tsukuba City (2012) events [26], [27]. A comma-shaped pattern was identified in a tornado event in the coastal area of the Sea of Japan.

A significant finding from CMAX signatures is the diversity of echo patterns associated with analyzed PB events, which ranged from classic hook echoes and bow echoes to linear and V-shape formations. This variability serves as a critical caution for operational forecasters: relying solely on the detection of a 'classic' supercellular hook echo is insufficient for PB monitoring in Indonesia. Adequate early warning requires a broadened focus that recognizes this spectrum of convective morphologies, rather than searching for a singular, idealized radar signature.

In southern Jiangsu, eastern China, a tornado that occurred on May 14, 2021, shows a hook echo pattern on weather radar images [29], [30]. Meanwhile, in the Kaiyuan region of East China, a V-shape pattern was identified in the tornado on July 3, 2019 [31]. While in Seoul, South Korea, the hook echo pattern was also detected on weather radar during the tornado event on June 10, 2014 [32]. In other tropical regions, such as Brazil and the United States, the hook echo pattern was also identified in the November 19, 2015, tornado event [33].

However, Indonesian PB events showed a more diverse pattern type, including bow and V-shape echoes, suggesting possible regional variations in formation mechanisms, potentially due to the unique maritime continent atmospheric dynamics. The reflectivity values (35–60 dBZ) observed in Indonesian PB events align with findings from China [21], India [34], South Africa [35], and U.S. non-supercell tornadoes [36]. However, they remain notably lower than those typically associated with U.S. supercell tornadoes (45–70 dBZ) [37].

It is also crucial to consider the instrumental characteristics of the C-band radar systems used in this study. In tropical environments characterized by intense rainfall, C-band signals are susceptible to attenuation, which can lead to an underestimation of the actual reflectivity values. Consequently, the observed CMAX range of 35–60 dBZ likely represents a conservative lower bound, and actual core intensities may be higher. This attenuation effect introduces a complicating factor in establishing a precise CMAX threshold, implying that while values greater than 35 dBZ are a useful baseline, forecasters should remain vigilant even if observed values do not reach the extreme levels typical of unattenuated measurements.

PB's signatures on HWIND. Based on the results of horizontal wind analysis at an altitude of 4 km from the surface in 10 PB cases, the wind speed ranges from 5 to 35 knots. The 4 km altitude was selected to characterize the mid-level environmental steering flow governing storm motion, distinct from the surface-based friction layer. However, it is important to acknowledge the inherent limitations of the HWIND product. This parameter is a retrieval derived from single-Doppler radial velocity data, not a direct measurement of the full horizontal wind vector. Unlike dual-Doppler syntheses, this method relies on assumptions of wind field uniformity within the analysis volume and therefore represents an estimated horizontal approximation. The dominant wind direction at 5 PB locations was from Northeast to Southeast, and 2 locations had a direction from West to Southwest. The maximum radar-detected radial velocity at the PB sites ranged from 20 to 30 knots. While these values are below the theoretical threshold for tornadic winds (>34 knots), they are consistent with the partial beam-filling effect observed in C-band radars, where the narrow vortex (<100m) is averaged against the wider radar beam (>1km). Therefore, a radar signature of 25-30 knots in this region should be interpreted as a potential proxy for significantly higher, unresolvable ground-level velocities.

The temporal pattern of the PB event was identified to have 3 phases: an intensification phase characterized by a sudden increase in wind speed, a peak phase with the persistence of high wind speed and relatively stable wind direction, and a weakening phase with a gradual decrease in wind speed.

Overall, from the analysis of HWIND products, the specific features for PB identification include a sudden increase in wind speed exceeding 20 knots, persistence of wind direction and speed in the peak phase for 10-20 minutes, and a gradual decrease in wind speed after the PB event. Figures 4a and 4b present images of the HWIND product at the Angkinang and Sintang PB locations.

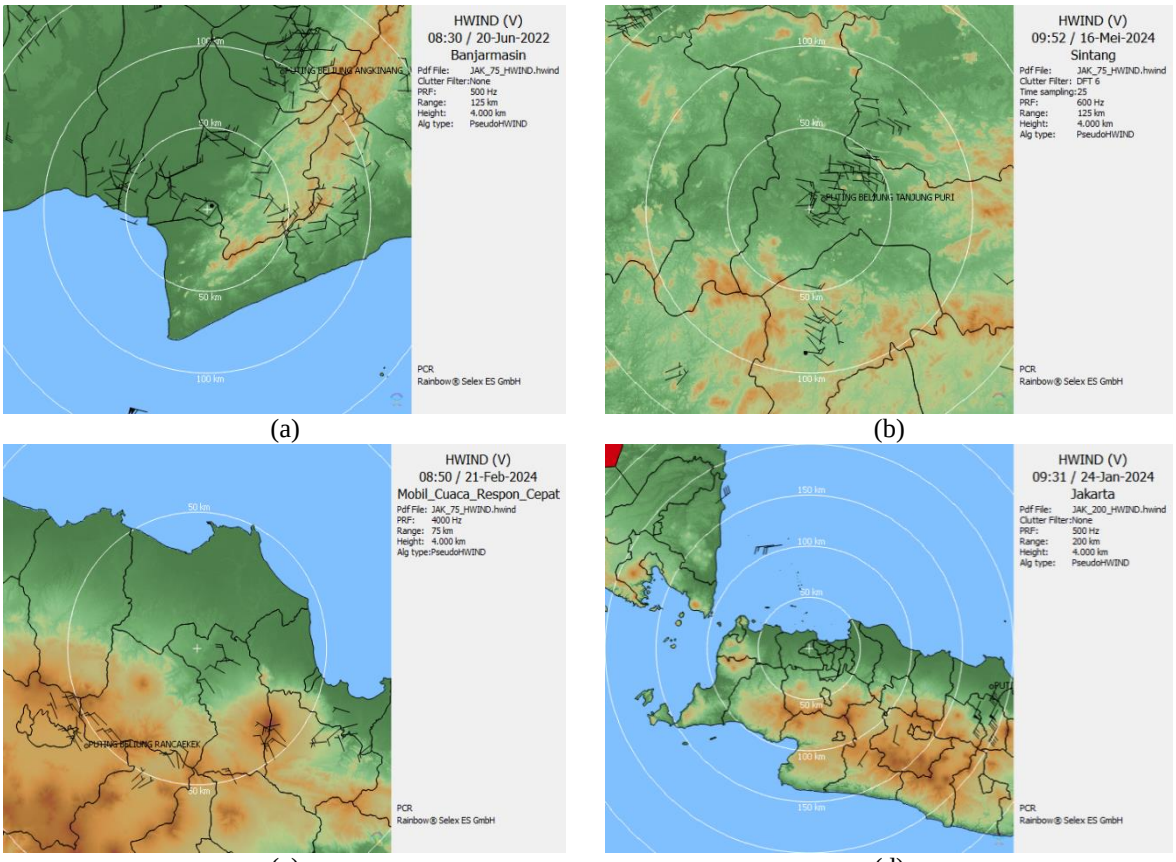

Figure 4. HWIND images of PB events at (a) Angkinang, Banjarmasin, South Borneo (b) Tanjung Puri, Sintang, West Borneo (c) Rancaekek, Bandung, West Java (d) Tukdana, Indramayu, West Java. Wind barbs indicate wind direction and speed, with the barbs pointing in the direction the wind blows.

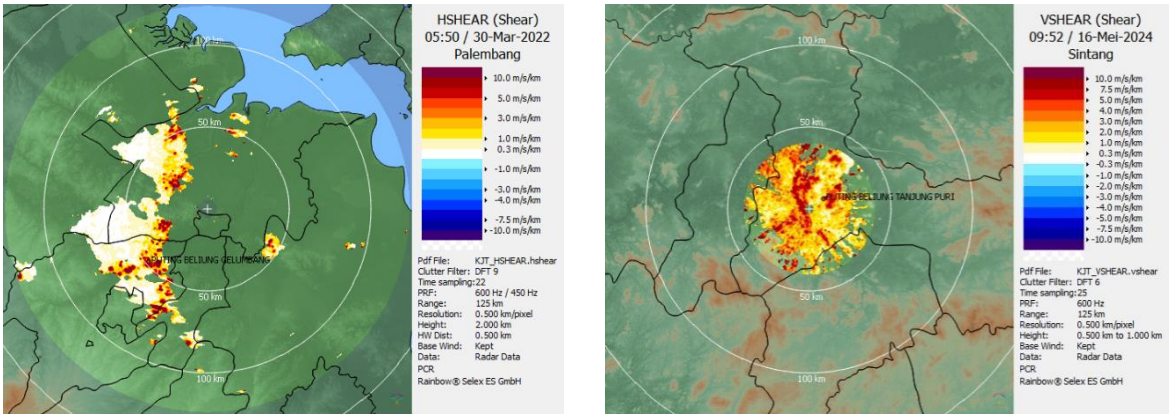

Figure 5. (a) Horizontal wind shear (HSHEAR) radar visualization from Gelumbang, Palembang, South Sumatra, on March 30, 2022, at 05:50 UTC (b) Vertical wind shear (VSHEAR) radar visualization from Tanjung Puri, Sintang, West Borneo, on May 16, 2024, at 09:52 UTC, the wind shear intensity color scale ranging from -10.0 m/s/km (dark blue) to 10.0 m/s/km (dark red).

PB's signatures on SHEAR. The horizontal shear products at the 10 PB locations were consistently identified at a 2 km altitude, with values ranging from 0.3 to 10 m/s/km, as seen at the Gelumbang PB site (Figure 5a). Quantitative analysis reveals that PB genesis is preceded by horizontal shear values of 5–10 m/s/km (0.005 - 0.010 s^{-1}). Notably, this range falls just below or at the lower threshold of the classic mesocyclone definition used in mid-latitude severe weather (>0.01 s^{-1}), suggesting that Indonesian PBs may be driven by local shearing instabilities (non-supercell processes) rather than deep, persistent mesocyclones. Furthermore, the detection of vertical shear in only 30% of cases—and exclusively at low altitudes (0.5–1.0 km), supports a 'bottom-up' formation mechanism, characteristic of landspout-type tornadoes. Crucially for early warning systems,

these shear signatures were consistently detectable approximately 30 minutes prior to touchdown.

PB's signatures on SPECTRAL WIDTH. Based on the spectral width (W) product analysis at 10 PB locations, index values ranging from 1 to 3 m/s were identified at an altitude of 500 meters. Spectral Width (W) analysis reveals values consistently ranging between 1.0 and 3.0 m/s across the precipitation field (Figures 6a, and 6b). While the PB location coincided with the upper end of this range (reaching 3.0 m/s), this signature provided low contrast against the ambient storm background, which also exhibited widths ranging from 1.0 to 3.0 m/s. This lack of a distinct high-magnitude spike (e.g., 4-8 m/s) confirms that Partial Beam Filling severely dilutes the turbulence signature of small-scale Indonesian vortices (PB). Consequently, while Spectral Width can serve as a secondary confirmation tool, it is less effective as a primary detection parameter for PB compared to Velocity or Shear products.

PB's signatures on SSA. Analysis of the CMAX product reveals peak reflectivity values that generally range from 35 to 60 dBZ during the mature phase. Interestingly, SSA (Storm Structure Analysis) identified slightly higher maximum point values (reaching 63 dBZ in the Rancaekek case as presented in Figures 7). This minor discrepancy indicates that the highest-intensity cores within Indonesian PB storms are likely extremely compact and transient, detected by the 3D cell-tracking algorithm (SSA) but spatially smoothed in the 2D CMAX projection.

Physically, this confirms that while the general storm envelope exhibits moderate intensity (35–60 dBZ, consistent with tropical warm rain), the storm core momentarily achieves severe-level intensity (>60 dBZ, indicative of mixed-phase ice) during the rapid 10–20 minutes growth phase. This 'pulse-like' intensification is a critical signature for early warning.

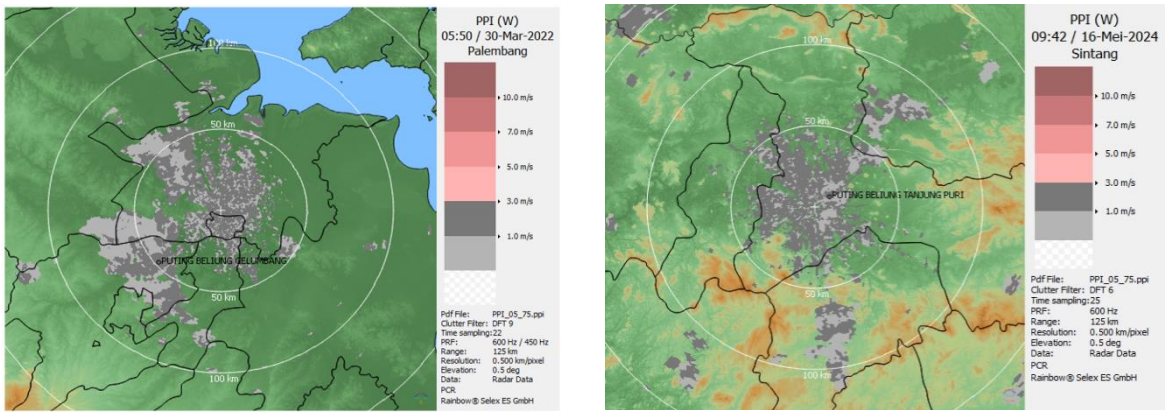

(a) (b)

Figure 6. PPI (Plan Position Indicator) radar visualization from (a) Gelumbang, Palembang, South Sumatra, on March 30, 2022, at 05:50 UTC (b) Tanjung Puri, Sintang, West Borneo, on May 16, 2024, at 09:42 UTC, the radar displays velocity data with a scale ranging from 1.0 m/s (gray) to 10.0 m/s (dark red), significant areas of spectral width indicated by gray shading.

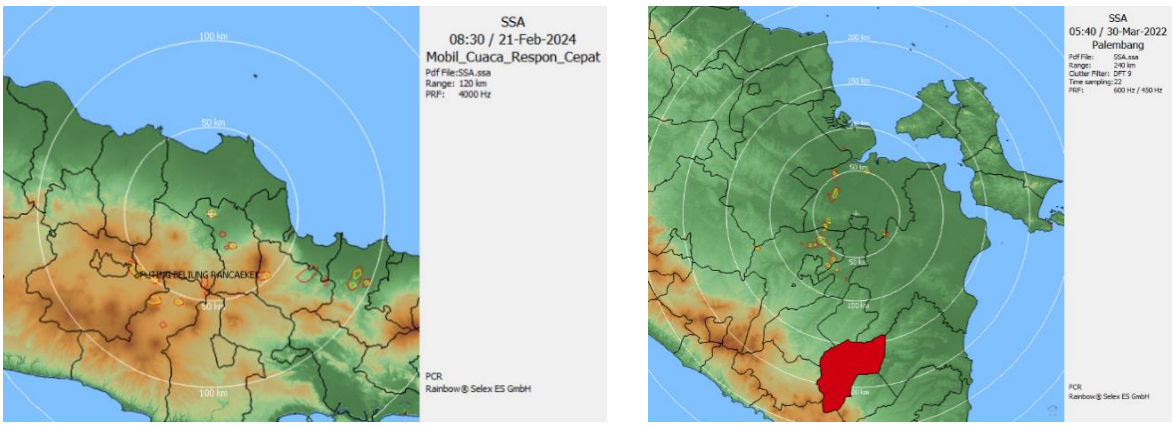

(a) (b)

Figure 7. SSA visualization of PB events at (a) Rancaekek, Bandung, West Java (b) Gelumbang, Muara Enim, South Sumatra. The red and yellow polygon represents the storm and the storm's core respectively.

The observation of 63 dBZ at an altitude of 8.7 km, well above the freezing level, strongly suggests the presence of large hail or graupel within a vigorous updraft, as liquid water is unlikely to sustain such high reflectivity at this altitude. This vertical structure indicates that the Rancaekek event departs significantly from the shallow, 'warm rain' mechanisms typical of tropical PBs. Instead, it exhibits severe supercellular or 'continental-like' characteristics, a conclusion that is further corroborated by the TVD finding of a deep rotational column extending to 3.1 km.

There is a variation in the dimensions of the storm cloud system with a diameter range of 5 to 51 km^2 and a volume range of 6 to 246 km^3. The largest cloud systems were observed in the cases of Rancaekek and Gelumbang PBs, while Belinyu PB showed the smallest cloud systems. The vertical growth of storm cloud systems also varied, with cloud base heights between 190 meters and 4 km (Rancaekek), and cloud top heights between 2.6 km (Tanjung Puri and Belinyu) and 11.4 km (Rancaekek). It should be noted that the lowest altitude observed for the Rancaekek storm was 2.6 km. This value corresponds to the radar-detected base determined by beam height limitations, rather than the true physical cloud base.

Temporal characteristics show that most PB cases exhibit rapid progression, although with varying durations. Rancaekek showed the longest-lasting system (more than 30 minutes), while Belinyu recorded the shortest time. The Storm Structure Analysis (SSA) reveals distinct morphological differences among PB-producing storms. While all cases exhibited core reflectivity greater than 50 dBZ, the Rancaekek case was anomalous, displaying 63 dBZ at an altitude of 8.7 km. This signature, indicative of mixed-phase ice processes and deep convection, contrasts sharply with the shallower cases (e.g., Belinyu, Top <3 km). This variance confirms that PB events in Indonesia arise from two distinct storm modes: deep, supercellular convection (characterized by volumes >200 km^3 and high-altitude cores) and shallow, pulse-like convection (volumes <20 km^3). Consequently, an SSA threshold of >50 dBZ serves as a necessary, but not sufficient, condition for a PB warning, with the vertical extent serving as the discriminator for event severity.

PB's signatures on TVD. The TVD product detects Tornado Vortex Signature (TVS), where the presence of TVS indicates a tornado [22], or in this case, a PB. Based on the analysis of TVD products at 10 PB locations, 6 locations show circulation, while 4 PB locations do not. All six locations show cyclonic circulation, the intensity of which varies from weak to strong categories. Rancaekek had the strongest circulation with horizontal shear at the surface reaching 26.1 m/s, while other PB sites showed weaker intensity with speeds ranging from 13.5 to 15.8 m/s, as shown in Figure 8a.

Rotation heights also vary, with Rancaekek having the highest rotation at 3.1 km, while the rotation system in Belinyu was recorded at 0.7 km. The majority of rotating systems were at heights between 1.2 and 2.3 km. Maximum wind speeds in the circulation area were identified at various heights in the 1.2 to 3.5 km range.

From a temporal perspective, the duration of circulation detection varies between PB cases. Some locations, such as Belinyu, show a fairly long detection period of more than 1 hour, while other locations, such as Rancaekek, are detected at shorter times. A key point is that the circulation location is not always precisely at the PB event site but is often detected in the surrounding area. Figure 8b presents the image of the TVD product at the Angkinang PB site.

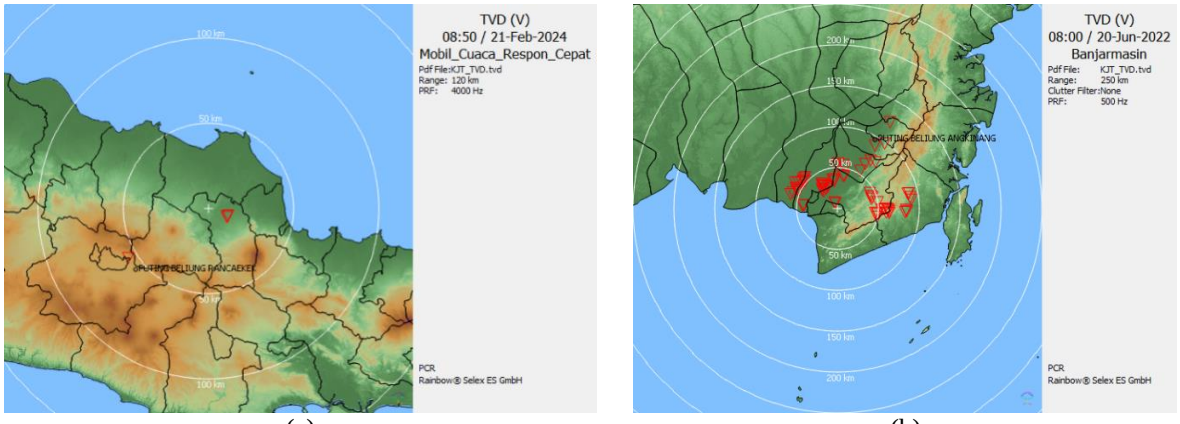

(a) (b)

Figure 8 TVD radar visualization from (a) MCRC radar from Rancaekek, Bandung, West Java, on February 21, 2024, at 08:50 UTC, (b) Angkinang, Banjarmasin, South Borneo, on June 20, 2022, at 08:00 UTC, the red triangle represents cyclonic circulation.

In the tornado events in Kaiyuan, on July 3, 2019, and in Suzhou City, China, on July 6, 2020, TVD products detected cyclonic circulation at altitudes up to 0.7 km above the surface [21], [31]. TVS products have also been utilized to analyze the rotational evolution of tornadoes in seven case studies across the United States [23]. The detection of circulation at altitudes of 1.2–3.1 km suggests that a subset of Indonesian PB events, particularly high-intensity cases, such as Rancaekek, possess deep, organized rotating updrafts akin to Mini-Supercells, rather than being limited to shallow, surface-based 'landspout' mechanisms. While Chinese studies reported lower detection heights (0.7 km), this discrepancy may partially result from radar sampling geometry (beam elevation at range). However, the presence of rotation extending above 3 km confirms that significant PB events involve deep-layer processes, challenging the assumption that all tropical tornadoes are shallow, non-mesocyclone features.

A notable finding of this study is the rapid development of Indonesian PB events. The cloud growth phase lasts approximately 10-20 minutes from initiation to maturity, with an average total lifecycle duration of 30-40 minutes. This is considerably shorter than the average duration of tornadoes in the United States, which typically ranges from 60 to 90 minutes [38]. This shorter duration highlights the urgent need for rapid detection and warning systems tailored to Indonesian conditions.

The observational results reveal a distinct pattern across ten analyzed PB cases, characterized by consistently moderate low-level horizontal shear (5–10 m s^{-1} km^{-1}) contrasting with inconsistent vertical shear and intermittent TVD identifications. Rather than indicating contradictory findings, we propose that this specific combination of signatures points to a predominant non-mesocyclonic or 'landspout-type' genesis mechanism for typical Indonesian *Puting Beliung* events. Unlike supercellular tornadoes driven by a 'top-down' dynamic piping process associated with a deep mesocyclone, these events likely follow a 'bottom-up' formation theory where pre-existing vertical vorticity along near-surface convergence boundaries, detected here as HShear, is stretched vertically by the developing updraft. This physical model successfully explains the disparities in product performance since HShear proves to be the most robust predictor by capturing the precursor boundary vorticity. In contrast, TVD and Vshear algorithms are less effective due to the absence of a deep and persistent mesocyclone. Furthermore, this mechanism aligns with the observed moderate to high CMAX values (35–60 dBZ) and rapid evolution phases, which are typical characteristics of vortices that spin up quickly in developing congestus or cumulonimbus clouds without the mature infrastructure of a supercell. Similar outcomes were described by Yao et al. [39], whose CM1 model simulations of tornadogenesis concluded that the process is characterized by the rapid upward growth of the tornado-scale vortex. This finding that aligns with the growing body of evidence supporting bottom-up vortex development.

Table 4 summarizes the quantitative values derived from the analysis and interpretation of weather radar products in the study's 10 case studies of PB events. Detailed radar-derived products for each of the ten analyzed PB cases are presented in the Supplementary Information to ensure a comprehensive representation of the dataset.

It is essential to note that the operational thresholds proposed in this study (Reflectivity > 35 dBZ, HWIND > 20 knots, HShear > 5 m/s/km) serve as a baseline for automated detection but are subject to radar resolution limitations. Our data showed PB events associated with radial velocities as low as 10 knots. These lower values are attributed to partial beam filling, where the small-scale tornado vortex is unresolved within the larger radar sampling volume, leading to velocity underestimation [40], [41].

Consequently, relying solely on a threshold of more than 20 knots may result in missed detections for smaller, weaker vortices. To mitigate this, we propose the tiered warning system, where pattern recognition (e.g., hook or bow echoes) complements quantitative thresholds. Future implementation should consider adaptive thresholds that adjust based on the storm's distance from the radar to account for beam broadening effects.

Table 4. Weather radar-derived product values at 10 PB case study events.

PB Case study /Radar-derived products	1	2	3	4	5	6	7	8	9	10	Comments
CMAX (dBZ)	50-60	45-60	50-60	45-55	45-50	45-60	45-50	45-50	35-40	35-40	Cases 1-3, 6 have high reflectivity (>50 dBZ), indicating strong convection. Cases 9-10 have lower values.
CMAX (Pattern)	-	V-shape	Bow echo	Hook echo	Hook echo	Line shape	-	-	-	-	Bow echo (case 3) and hook echoes (cases 4-5) suggest potential severe weather/PB.
HWIND (Direction)	NE	NW-SE	E	E	NE	W	-	NE	SW	S	Wind directions vary, with NE being dominant. Case 2 has shifting winds (NW-SE).
HWIND Windspeed (knots)	25	20	20	20	10	30	-	10	15	30	Strongest winds in cases 6 and 10 (30 knots). Cases 5, 8 show weaker winds (≤10 knots).
SHEAR (Horizontal m/s/km)	5-10	0-5	5-10	5-10	7.5-10	7.5-10	-	1-5	5-10	-	Cases 3-6 and 9 have moderate shear (≥5 m/s/km), supporting storm organization.
SHEAR (Vertical m/s/km)	-	-	5-10	5-10	-	-	-	1-5	-	-	Only cases 3, 4, and 8 have vertical shear, indicating potential updraft tilting.
SPECTRAL WIDTH (m/s)	3	3	3	3	3	3	3	1	3	1	Generally moderate spectral width (3 m/s), suggesting small-scale turbulence.
SSA (Extent km^2)	-	51	22	-	5	45	5	5	-	12	The largest SSA extents are in cases 2 and 6, indicating broader storm coverage.
SSA (Volume km^3)	-	246	20	-	6	129	9	5	-	35	Case 2 has the highest volume (246 km^3), likely indicating a larger storm system.
SSA (Max Z dBZ)	-	63	56	-	52	61	51	48	-	49	The highest SSA reflectivity in cases 2 and 6 (≥60 dBZ) was is linked to strong convection.
TVD (Rotation height km)	1.7	3.1	-	1.6	1.2	1.3	-	-	1.6	-	Rotation heights vary (1.2–3.1 km), with case 2 having the highest rotation.

4. Conclusion

The analysis demonstrates that most Puting Beliung (PB) cases in Indonesia exhibit moderate to high reflectivity values (35–60 dBZ) with diverse echo patterns, ranging from classic hook echoes to bow echoes, V-shapes, and line formations. A critical operational finding is the extremely rapid lifecycle of these events, characterized by a growth phase of only 10–20 minutes. Regarding kinematic signatures, Horizontal Wind speeds generally varied between 10 and 30 knots. Notably, Horizontal Shear (HShear) emerged as the most consistent predictor, with values consistently exceeding 5 m s^{-1} km^{-1}. In contrast, Vertical Shear and Tornadic Vortex Detection (TVD) signatures were less consistent, identified in only 30% and 60% of cases, respectively. This disparity—where low-level boundary shear dominates over deep-layer rotation—suggests that many Indonesian PB events may follow a non-mesocyclonic ('landspout-type') genesis mechanism, distinct from the classic supercellular processes often detected by TVD.

Based on these findings, we propose several operational implications for the detection of PB. Given the absence of a non-tornadic 'null dataset' in this study, the False Alarm Rate (FAR) remains unknown. Therefore, we propose the following criteria as preliminary thresholds for further operational testing rather than definitive rules: reflectivity > 35 dBZ, Horizontal Wind > 20 knots, and HShear > 5 m s^{-1} km^{-1}. These parameters show promise as effective 'first-look indicators' within a tiered warning system: Level 1 for detecting favorable conditions, Level 2 for recognizing echo formations, and Level 3 for confirming rotation. Considering the observed rapid growth phase, a warning lead time of 15–20 minutes is recommended as a realistic maximum target for this phenomenon.

Future research should focus on validating these thresholds against non-tornadic datasets to refine their discrimination capability and reduce false alarms. Additionally, technical development should prioritize machine learning algorithms for PB detection. Approaches such as Convolutional Neural Networks (CNN) [42], Support Vector Machines (SVM) [43], Random Forest [15], and Multi-Head Convolutional Block (MHCB) [20] methods could substantially enhance identification speed and accuracy. By automating the detection of these specific radar signatures, forecasters can issue more timely warnings, potentially mitigating the impact of these rapid-onset catastrophic events.

Acknowledgement

The authors thank the Indonesia Endowment Fund for Education (LPDP) for providing financial support for this research through the 2024 research funding scheme.

References

[1] BNPB, “Statistik Bencana Menurut Jenis,” 2024. [Online]. Available: https://dibi.bnpb.go.id/kbencana2

[2] BMKG, “Prosedur Standar Operasi Pelaksanaan Peringatan Dini Pelaporan dan Diseminasi Informasi Cuaca Ekstrim,” p. 3, 2010.

[3] S. Lee, J. Kim, Y. Maharani, E. Paripurno, and Sunaryo, “Analysis of the Risk of Windstorm (angin puting beliung) in Indonesia,” *J. Wind Eng. Inst. Korea*, vol. 2, no. 1, pp. 21–28, 2017.

[4] S. Mujiasih, S. T. Primadi, S. Si, J. R. Tuban, and K. Badung, “Analisis Kejadian Puting Beliung Tanggal 11 Desember 2013 Di Wilayah Denpasar Bagian Selatan,” *Pros. Work. Radar dan Satelit Cuaca*, vol. II, pp. 117–122, 2014.

[5] E. Yulihastin, “A High Wind Associated with Bow Echo Mesovortex over Cimenyan , Indonesia,” *Res. Sq.*, pp. 1–24, 2023, [Online]. Available: chrome-extension://kdpelmjpfafjppnhbloffcjpeomlnpah/https://assets-eu.researchsquare.com/files/rs-3424786/v1/f6605e16-c931-48c5-95ea-93d0e1737963.pdf?c=1696963825

[6] E. Nurjani, A. Rahayu, and F. Rachmawati, “Kajian Bencana Angin Ribut Di Indonesia Periode 1990-2011: Upaya Mitigasi Bencana,” *Geomedia Maj. Ilm. dan Inf. Kegeografian*, vol. 11, no. 2, pp. 191–206, 2013, doi: 10.21831/gm.v11i2.3451.

[7] R. Darman, “Analisis Data Kejadian Bencana Angin Puting Beliung Dengan Metode Online Analytical Processing (Olap),” *SINTECH (Science Inf. Technol. J.*, vol. 2, no. 1, pp. 18–23, 2019, doi: 10.31598/sintechjournal.v2i1.298.

[8] A. Ali and S. Hidayati, “Whirl Wind Detection and Identification in Indonesia Utilizing Single Polarization Doppler Weather Radar Volumetric Data,” *Int. Arch. Photogramm. Remote Sens. Spat. Inf. Sci. - ISPRS Arch.*, vol. 41, no. July, pp. 1221–1227, 2016, doi: 10.5194/isprsarchives-XLI-B8-1221-2016.

[9] T. Nurlambang *et al.*, “Penanggulangan Bencana Cuaca Ekstrim di Indonesia,” *Pros. Semin. Nas. Ris. Kebencanaan*, pp. 1–8, 2013.

[10] K. Kiki, Y. Koesmaryono, R. Hidayat, D. S. Permana, and P. Perdinan, “Spatiotemporal Characteristics and Trend of Puting Beliung Across the Indonesian Archipelago,” vol. 57,

pp. 334–346, 2025, doi: 10.22146/ijg.103901.
[11] T. Aliftha, A. Azwar, and R. Adriat, "Penerapan Metode Analisis Diskriminan terhadap Variasi Unsur Cuaca pada Kejadian Puting Beliung di Jawa Tengah," *Prism. Fis.*, vol. 8, no. 1, pp. 57–61, 2020, doi: 10.26418/pf.v8i1.40174.
[12] G. R. Nikmah and H. Hazim, "Gambaran Kecemasan Masyarakat Desa X Di Sidoarjo Pasca Bencana Angin Puting Beliung," *J. Mhs. BK An-Nur Berbeda, Bermakna, Mulia*, vol. 9, no. 3, pp. 150–156, 2023, doi: 10.31602/jmbkan.v9i3.12054.
[13] E. De Lima Nascimento, G. Held, and A. M. Gomes, "A multiple-vortex tornado in Southeastern Brazil," *Mon. Weather Rev.*, vol. 142, no. 9, pp. 3017–3037, 2014, doi: 10.1175/MWR-D-13-00319.1.
[14] M. S. Veillette, J. M. Kurdzo, P. M. Stepanian, J. Y. N. Cho, S. Samsi, and J. McDonald, "A Benchmark Dataset for Tornado Detection and Prediction using Full-Resolution Polarimetric Weather Radar Data," pp. 1–37, 2024, [Online]. Available: http://arxiv.org/abs/2401.16437
[15] Q. Zeng *et al.*, "Application of Random Forest Algorithm on Tornado Detection," *Remote Sens.*, vol. 14, no. 19, pp. 1–22, 2022, doi: 10.3390/rs14194909.
[16] L. G. Gmbh, "Software Manual Rainbow ® 5 Products & Algorithms Guide," 2023, [Online]. Available: www.leonardogermany.com
[17] I. Rusmala, R. Zikri, R. N. Rahman, M. I. R. Ansori, I. R. Nugraheni, and A. Ali, "Identification of Small Tornado Event Using Weather Radar and Himawari-8 Products (Case Study : Puting Beliung Event on November 22 , 2018 in Jakarta)," *Spec. Issue 2nd Int. Conf. Trop. Meteorol. Atmos. Sci.*, pp. 15–20, 2022.
[18] I. J. A. Saragih *et al.*, "Utilization of Red-Green-Blue (RGB) modification composite for nighttime convective cloud monitoring over North Sumatra region," *IOP Conf. Ser. Earth Environ. Sci.*, vol. 893, no. 1, 2021, doi: 10.1088/1755-1315/893/1/012019.
[19] R. D. Yudistira *et al.*, "Utilization of surface meteorological data, Himawari-8 satellite data, and radar data to analyze landspout in Sumenep, East Java, Indonesia (case study of 20 November 2017)," *IOP Conf. Ser. Earth Environ. Sci.*, vol. 374, no. 1, 2019, doi: 10.1088/1755-1315/374/1/012038.
[20] J. Xie *et al.*, "Multi-Task Learning for Tornado Identification Using Doppler Radar Data," *Geophys. Res. Lett.*, vol. 51, no. 11, 2024, doi: 10.1029/2024GL108809.
[21] S. Cao, Y. Wang, G. He, P. Shen, Y. He, and Y. Wu, "Radar Characteristics and Causal Analysis of Two Consecutive Tornado Events Associated with Heavy Precipitation during the Mei-Yu Season," *Remote Sens.*, vol. 15, no. 23, pp. 1–22, 2023, doi: 10.3390/rs15235470.
[22] R. A. Brown and V. T. Wood, "Detection of the presence of tornadoes at the center of mesocyclones using simulated Doppler velocity measurements," *Weather Forecast.*, vol. 30, no. 4, pp. 957–963, 2015, doi: 10.1175/WAF-D-15-0014.1.
[23] J. L. Houser, H. B. Bluestein, K. Thiem, J. Snyder, D. Reif, and Z. Wienhoff, "Additional Evaluation of the Spatiotemporal Evolution of Rotation during Tornadogenesis Using Rapid-Scan Mobile Radar Observations," *Mon. Weather Rev.*, vol. 150, no. 7, pp. 1639–1666, 2022, doi: 10.1175/MWR-D-21-0227.1.
[24] Y. Wang, T. Wang, P. Yang, and W. Xue, "A Numerical Simulation of the '1907' Kaiyuan Tornado Weather Process in Liaoning, Northeast China," *Atmosphere (Basel).*, vol. 13, no. 2, 2022, doi: 10.3390/atmos13020219.
[25] M. M. French, P. S. Skinner, L. J. Wicker, and H. B. Bluestein, "Documenting a rare Tornado merger observed in the 24 May 2011 El Reno-Piedmont, Oklahoma, Supercell," *Mon. Weather Rev.*, vol. 143, no. 8, pp. 3025–3043, 2015, doi: 10.1175/MWR-D-14-00349.1.
[26] W. Mashiko, "A numerical study of the 6 May 2012 Tsukuba City Supercell Tornado. Part II: Mechanisms of tornadogenesis," *Mon. Weather Rev.*, vol. 144, no. 9, pp. 3077–3098, 2016, doi: 10.1175/MWR-D-15-0122.1.
[27] F. Kobayashi, Y. Sugawara, M. Imai, M. Matsui, A. Yoshida, and Y. Tamura, "Tornado generation in a narrow cold frontal rainband - Fujisawa tornado on April 20, 2006 -," *Sci. Online Lett. Atmos.*, vol. 3, pp. 21–24, 2007, doi: 10.2151/sola.2007-006.
[28] H. Y. Inoue *et al.*, "Finescale doppler radar observation of a tornado and low-level misocyclones within a winter storm in the Japan Sea coastal region," *Mon. Weather Rev.*, vol. 139, no. 2, pp. 351–369, 2011, doi: 10.1175/2010MWR3247.1.
[29] B. Wu, M. Wei, and Y. Li, "Dual-Polarization Radar Observations of the Evolution of a Supercell Tornado and Analysis of the Echo Mechanisms," *Atmosphere (Basel).*, vol. 13, no. 5, pp. 1–17, 2022, doi: 10.3390/atmos13050797.
[30] Y. Li, S. Cao, X. Wang, and L. Wang, "Comparative Analysis of Two Tornado Processes in Southern Jiangsu," *Atmosphere*

(Basel)., vol. 2, 2024, doi: https://doi.org/10.3390/atmos15081010.

[31] Y. Wang, T. Wang, P. Yang, and W. Xue, "A Numerical Simulation of the '1907' Kaiyuan Tornado Weather Process in Liaoning, Northeast China," *Atmosphere (Basel).*, vol. 13, no. 2, 2022, doi: 10.3390/atmos13020219.

[32] S. Lim, S. Allabakash, B. Jang, and V. Chandrasekar, "Polarimetric radar signatures of a rare tornado event over South Korea," *J. Atmos. Ocean. Technol.*, vol. 35, no. 10, pp. 1977–1997, 2018, doi: 10.1175/JTECH-D-18-0041.1.

[33] F. Vanessa, G. Vitor, and N. Ernani de Lima, "An environmental and polarimetric study of the 19 November 2015 supercell and multiple-vortex tornado in Marechal Cândido Rondon, southern Brazil," *Meteorol. Atmos. Phys.*, vol. 134, p. 82, 2022.

[34] M. K. Das, S. Das, M. A. M. Chowdhury, and S. Karmakar, "Simulation of tornado over Brahmanbaria on 22 March 2013 using Doppler weather radar and WRF model," *Geomatics, Nat. Hazards Risk*, vol. 7, no. 5, pp. 1577–1599, 2016, doi: 10.1080/19475705.2015.1115432.

[35] L. E. Lekoloane *et al.*, "A dynamic and thermodynamic analysis of the 11 December 2017 tornadic supercell in the Highveld of South Africa," *Weather Clim. Dyn.*, vol. 2, no. 2, pp. 373–393, 2021, doi: 10.5194/wcd-2-373-2021.

[36] J. S. Goodnight, D. A. Chehak, and R. J. Trapp, "Quantification of QLCS Tornadogenesis, Associated Characteristics, and Environments across a Large Sample," *Weather Forecast.*, vol. 37, no. 11, pp. 2087–2105, 2022, doi: 10.1175/waf-d-22-0016.1.

[37] C. N. Satrio, D. J. Bodine, R. D. Palmer, and C. M. Kuster, "Multi-radar analysis of the 20 may 2013 moore, oklahoma supercell through tornadogenesis and intensification," *Atmosphere (Basel).*, vol. 12, no. 3, pp. 1–30, 2021, doi: 10.3390/atmos12030313.

[38] J. Wang, J. Fan, and Z. Feng, "Climatological occurrences of hail and tornadoes associated with mesoscale convective systems in the United States," *Nat. Hazards Earth Syst. Sci.*, vol. 23, no. 12, pp. 3823–3838, 2023, doi: 10.5194/nhess-23-3823-2023.

[39] D. Yao, Z. Meng, and M. Xue, "Genesis, maintenance and demise of a simulated tornado and the evolution of its preceding descending reflectivity core (DRC)," *Atmosphere (Basel).*, vol. 10, no. 5, 2019, doi: 10.3390/atmos10050236.

[40] C. B. Griffin, D. J. Bodine, J. M. Kurdzo, A. Mahre, and R. D. Palmer, "High-temporal resolution observations of the 27 May 2015 Canadian, Texas, Tornado using the atmospheric imaging radar," *Mon. Weather Rev.*, vol. 147, no. 3, pp. 873–891, 2019, doi: 10.1175/MWR-D-18-0297.1.

[41] M. M. French, H. B. Bluestein, I. Popstefanija, C. A. Baldi, and R. T. Bluth, "Reexamining the vertical development of tornadic vortex signatures in supercells," *Mon. Weather Rev.*, vol. 141, no. 12, pp. 4576–4601, 2013, doi: 10.1175/MWR-D-12-00315.1.

[42] R. Lagerquist, A. McGovern, C. R. Homeyer, D. J. Gagne, and T. Smith, "Deep learning on three-dimensional multiscale data for next-hour tornado prediction," *Mon. Weather Rev.*, vol. 148, no. 7, pp. 2837–2861, 2020, doi: 10.1175/MWR-D-19-0372.1.

[43] V. A. Gensini, C. Converse, W. S. Ashley, and M. Taszarek, "Machine Learning Classification of Significant Tornadoes and Hail in the United States Using ERA5 Proximity Soundings," *Weather Forecast.*, vol. 36, no. 6, pp. 2143–2160, 2021, doi: 10.1175/WAF-D-21-0056.1.